Chapter 6:

Characterisation of Molecules in MCM-41 Channels

"Under the most rigorously controlled conditions of pressure, temperature, humidity, and other variables, the organism will do as it damn well pleases."

Anon.

The observation of molecular clusters has been of interest for some time. Molecular clusters can show quite different dynamic and static phase behaviour from bulk systems, and, because of their limited size, are accessible to computational molecular dynamics techniques.[1-3] Experimentally, molecular clusters are made using several methods, including supersonic jets, vapours, confinement of phases in emulsion droplets, condensation on surfaces and condensation in pores.[1]

The pore system of MCM-41 has previously been used to produce nanophase particles of platinum[4,5] cobalt,[6] binary caesium-lanthanum oxide clusters[7] and manganese-oxo species,[8] for catalysis purposes, and as a substrate for the creation of molecular wires.[9,10] The effects of confinement in the mesopores were studied only in relation to the molecular wires. It was found that polyaniline chains polymerised in MCM-41 channels were more conductive than similar chains polymerised in smaller, zeolite channels where inter-chain interactions were inhibited.[11] Some investigation of the properties of confined particles was carried out for semiconducting iron oxide particles.[12] The effect of confinement in uniform mesopores in that case was to produce a much wider bandgap, due to the quantum size effect, than had been previously seen for such materials. It has also been shown that the properties of polymers confined in the pores of MCM-41 differ from those in the bulk. The molecular weight has been observed to increase for poly(methyl methacrylate)[13] polymerised within the mesopores, and the glass transition temperatures of poly(vinyl acetate)[13] and polystyrene[14] has been shown to decrease with increasing confinement in MCM-41 materials.

Here the condensation of methane and hydrogen in the pores of MCM-41 results in mesoscale molecular structures which can be characterised by the use of gas isotherms, quasielastic neutron scattering and inelastic neutron scattering, and which show phase

behaviour which differs from that of bulk samples. Gases adsorbed in MCM-41 which have been studied by other workers include nitrogen,[15-17] argon,[18] cyclohexane,[19,20] benzene[21] and water.[22] In these cases the gas adsorption was used to characterise the MCM-41 pore system, not to observe changes in the behaviour of the adsorbate.

6.1 Methane in MCM-41

The experiments investigating the behaviour of methane in MCM-41 studied the capillary melting[23,24] of the methane and the phase transitions of a molecular solid and liquid absorbed in these narrow pores. This allowed some examination of the effect of small particle size in two dimensions upon the phase behaviour of methane. These experiments were done using early MCM-41 samples with low long range order.

The mesopores can be conveniently loaded to monolayer or multilayer coverage by equilibrating the outgassed silicate with appropriate doses of methane. When methane is present its scattering completely dominates that from the host lattice, owing to the large neutron-scattering incoherent cross-section of hydrogen compared to that of the other atoms present (see Table 3.1). The rotational dynamics of adsorbed methane in both tunnelling and librational energy ranges have provided much information on two dimensional phases and phase melting in other systems.[25-27]

6.2 Quasielastic Neutron Scattering from Methane

6.2.1 Background

The sample of MCM-41 used was prepared by the method of Beck *et al.*[28] The BET surface area from nitrogen adsorption was about 1,000 $m^2\ g^{-1}$. For the neutron scattering experiments the sample was outgassed at 250˚C with pumping to 10^{-5} torr for about 12 hours. It was then heated for three hours at 350˚C at 10^{-5} torr before being transferred into the aluminium sample container under an atmosphere of pure helium. The sample was filled with methane at 760 torr, sample temperature 140 K, that is, well above the condensation temperature of liquid methane and 6.68 mmol g^{-1} of methane were taken up.

The MCM-41 sample would have been extensively dehydrated by the vacuum and high temperature treatment applied before the filling with methane. It, nevertheless, contained surface hydroxyl groups arising from incomplete condensation of the polysilicate anions involved in the synthesis process. No attempt was made in this experiment to remove these either by deuterium exchange or ammoniation. These residual hydroxyl groups were responsible for a temperature dependent intensity variation in the quasielastic scattering from the empty MCM-41 sample shown in Figure 6.1. This background was taken into account in the analysis of the methane scattering data.

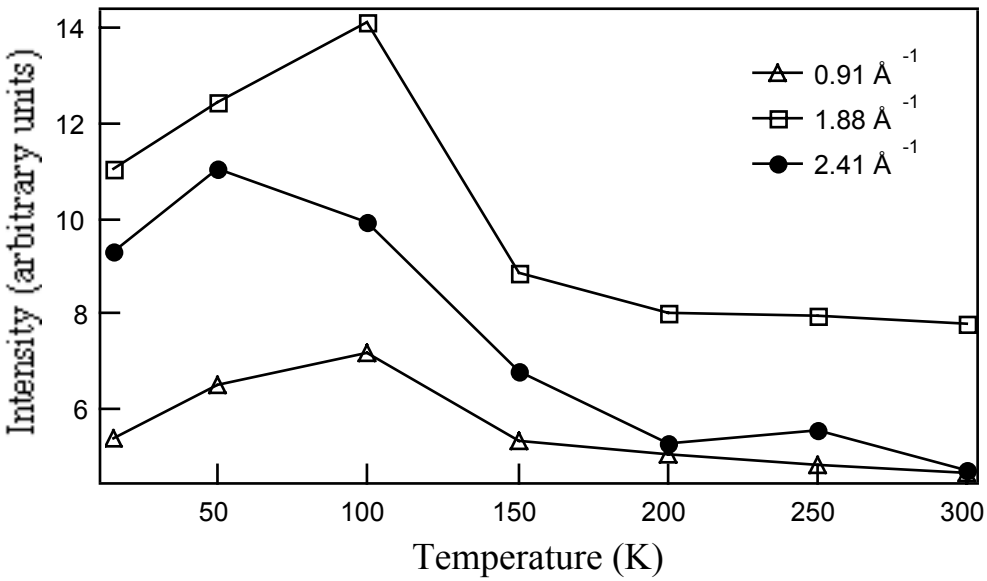

Figure 6.1 *Temperature dependence of the quasielastic scattering from the empty MCM-41 sample at several scattering angles.*

The quasielastic scattering was measured on the QENS instrument at the Intense Pulsed Neutron Source described in Chapter 3. There were clear changes in the elastic scattering intensity and the momentum transfer (Q) dependence of the quasielastic broadening with temperature between 15 and 180 K. These show that a modified phase behaviour for the adsorbed methane has arisen from the confinement in the channel system. Neutron scattering experiments on the outgassed MCM-41 from 15 to 300 K, were also carried out to ensure that any inelastic scattering from the siloxyl groups was accounted for, and also to define the elastic resolution function of the instrument. The resolution was found to be about 80 microelectron volts* over a momentum transfer, Q, range of $0.3 < Q < 2.6$ Å^{-1}. The resolution of the instrument did not allow clear observation of excitations below *ca* 100 microelectron volts (μeV) and no definite conclusions could be made on the existence of tunnelling. Data from bulk methane were taken with the same apparatus in a subsequent experiment as a control.

The quasielastic scattering functions from methane-filled MCM-41 such as that shown in Figure 6.2, were fitted with a delta function and the minimum number of Lorentzian components by a least squares method. Usually only one Lorentzian was required. The intensities of the Lorentzian and delta function components of the quasielastic peak were used to determine the elastic incoherent structure factors, EISF.[29] In addition, the energy widths of the Lorentzian components were determined.

* *Note: 1eV = 8068 cm^{-1}.*

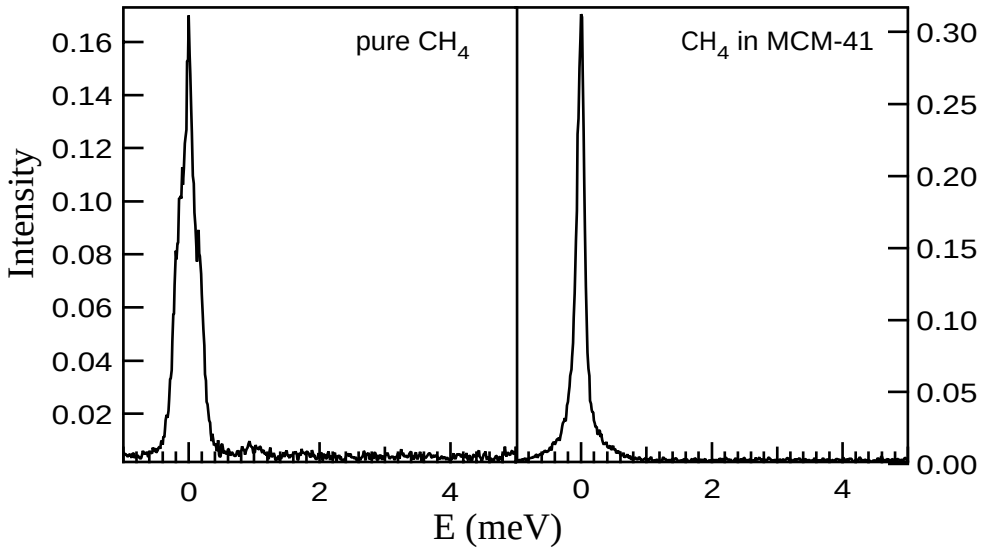

Figure 6.2 *Quasielastic scattering spectra for bulk methane at 15 K, Q = 2.41 Å^{-1} and for MCM-41 filled with 6.68 mmol g^{-1} of methane at the same temperature and scattering angle.*

In bulk methane, the face centred cubic solid structure is in an orientationally disordered plastic phase in the region below its melting point, down to T_c=20.4 K, where it undergoes a transition into the partially ordered structure of CH_4-II.[30,31] In this phase 75% of the molecules are orientationally ordered and librate about the minima of a strong anisotropic potential, while the other 25% are orientationally disordered. In the spectra of CH_4-II tunnelling peaks are expected at 75 μeV and 145 μeV, while a higher energy excitation, due to the almost free rotation of the disordered methane molecules, occurs at 1.07 meV.[31-33] In Figure 6.2 above the spectra collected for pure CH_4 at 15 K and Q = 2.41 Å^{-1} is shown. The peak at 1.07 meV can be seen, but the tunnelling lines are visible only as a distortion of the quasielastic peak centred around zero energy transfer, since the resolution is not sufficient to distinguish them at this temperature.

6.2.2 Results

The "window method" in quasielastic neutron scattering is a sensitive method of detecting transitions involving distinct changes in hydrogen motion, such as from rigid to rotator phase solids, as well as liquefaction. Figure 6.3 shows the temperature dependence of the quasielastic scattering intensity within the 80 μeV resolution "window" of the spectrometer for three different angles of scattering. The intensity drops each time the energy breadth of a newly activated dynamical process extends outside the "window". Here, it falls strongly between 60 and 120 K, indicating the onset of some new dynamic process in that temperature range. This phase transition might be relatively broad, but more experiments with higher resolution and a finer grid of temperatures would be needed to ascertain the degree to which the transition in this system has become continuous.

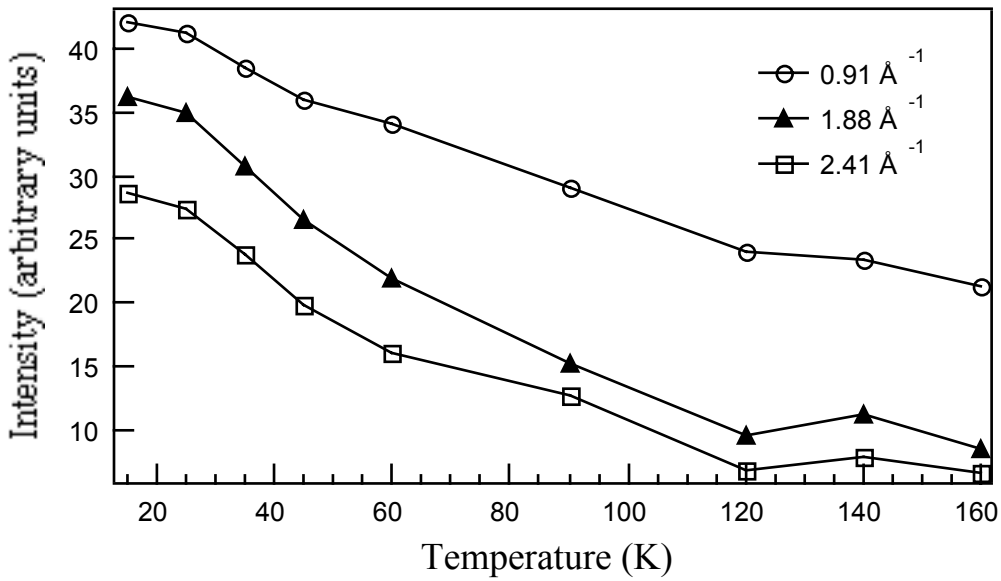

Figure 6.3 *Temperature dependence of the quasielastic scattering intensity at zero energy transfer for 6.68 mmol g^{-1} of methane in MCM-41, observed at various Q values.*

Figure 6.3 also shows that there is also a strong dependence of the total intensity on momentum transfer. This suggests that diffusion is associated with the transition observed in the intensity changes shown there. Vibration alone is unlikely to involve the large amplitude hydrogen motion that such a strong Q dependence implies. The momentum transfer dependence of the quasielastic broadening at various temperatures allows the transition seen by the "window method" to be assigned to diffusion. The melting point for bulk methane has been measured to be 91 K.[34] A reasonable inference, is therefore that the transition observed between 60 and 120 K is from rotational to translational diffusion. The elastic incoherent structure factors as a function of temperature, a more revealing observable, have been analysed and are shown in Figure 6.4.

From Figure 6.4 it is clear that the behaviour of the methane molecules in the MCM-41 channels is much the same for temperatures between 15 and 60 K. The slight increase in the EISF with increasing temperature is opposite to that observed in other systems. In those cases, a decrease in the EISF with increasing temperature was ascribed to jump rotational diffusion between inequivalent sites.[35,36] The small change seen here may be within the error of the measurements. However, there is also clearly a larger change in the methane behaviour which occurs between 60 and 90 K. The EISF decreases as the temperature increases, and the slope of the plot become much less. Large decreases in the EISF with temperature for water adsorbed in anionic clays have been assigned to the onset of haphazard large-scale movement of the water molecules.[36] Similar motions may be occurring here. The change in shape indicates a change from rotational diffusion to translational diffusion, for at least some of the molecules. By 160 K it can be seen that the shape of the EISF has completely changed. By this temperature, 50 K above the melting point of bulk methane at 112 K, most of the molecules in the MCM-41 channels would be undergoing translational diffusion.

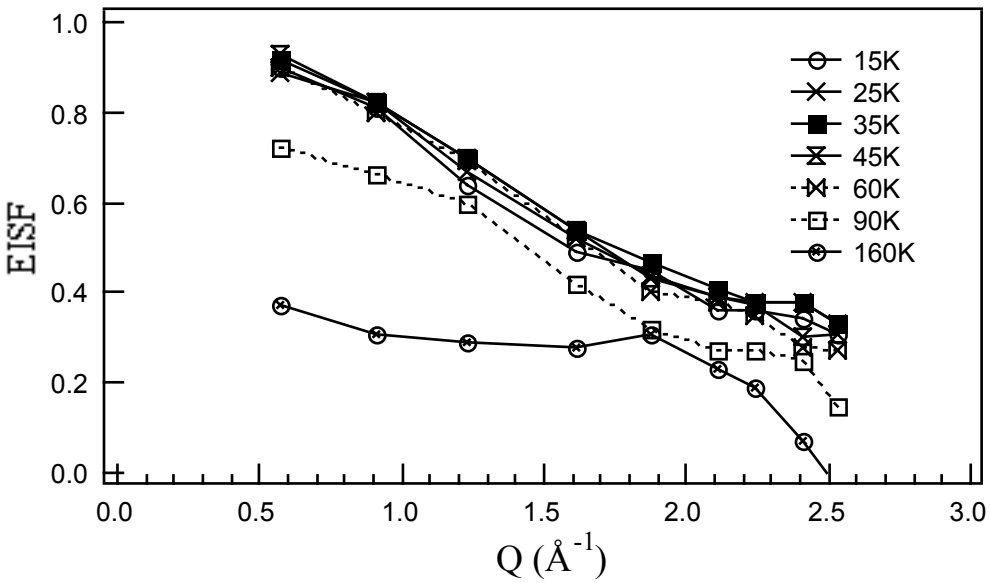

Figure 6.4 *Elastic incoherent structure factors for 6.68 mmol g^{-1} methane in MCM-41 at various temperatures.*

The EISF may also give further information concerning the type of rotational motion occurring at the lower temperatures through modelling of the fall-off with Q. Figure 6.5 below shows several models from the literature compared with the data taken at 15 K. The first model, isotropic rotation of the methane hydrogens on the surface of a sphere, has been found previously to describe the motion of methane in silicalite at 300 K.[37] The radius of the sphere was taken to be the C-H bond length in methane, 1.09 Å. The expected value of the EISF for such motion is then:

$$EISF = j_0^2(Q.r) \qquad \textbf{(6.1)}$$

where $j_0^2(Qr)$ is the zeroth order spherical Bessel function, and r is the radius of the sphere. This curve is shown in Figure 6.5 labelled as "isotropic."

The second model corresponds to jump diffusion of the methane hydrogens between two sites on a circle, 180˚ apart, in a powder sample with no favoured orientations.[38] It has been used to describe cases where a nucleus flips from side to side. The equation for this motion is:

$$EISF = \tfrac{1}{2} + \tfrac{1}{2}\frac{\sin(2Qr)}{2Qr} \qquad \textbf{(6.2)}$$

In this case 2r is the distance between the two sites is taken to have the same value as for equation 6.1 above. The resulting curve is plotted in Figure 6.5 as "2 sites."

The final model assumes a situation where some (65%) of the methane molecules are fixed, undergoing no rotational diffusion, but 35% are rotating isotropically. The EISF for this case is given by:

$$EISF = 0.39 + 0.65 j_0^2(Qr) \qquad \textbf{(6.3)}$$

The curve is plotted in Figure 6.5 as "39% static, 61% mobile."

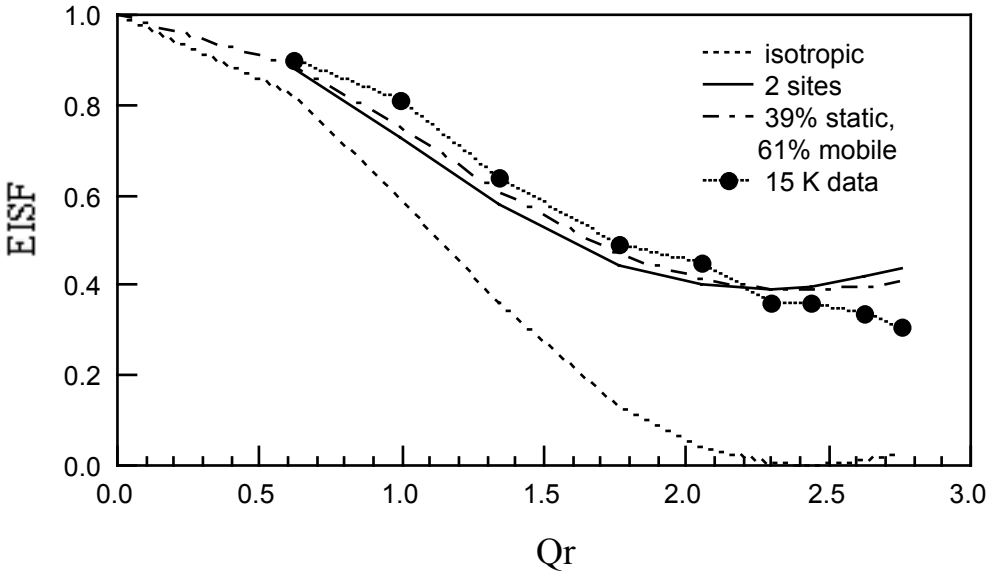

Figure 6.5 *The EISF for various models of rotational diffusion - isotropic motion on the surface of a sphere, jump diffusion between two sites 180˚ apart and a combination of static and rotationally active molecules. The experimental EISF measured at 15 K is shown for comparison.*

From Figure 6.5 it can be seen that the isotropic rotation model does not compare well with the data. The jump model over two sites is a reasonable fit to the observed EISF at 15 K, but the combination of static and rotationally active molecules is a slightly better fit. It is difficult to imaging why a rotating methane molecule might have two preferential sites for jump transitions. A three-site jump rotation model falls between the two-site model and the unhindered isotropic rotation model and so is clearly not a good description of the data. A combination of some molecules which are strongly hindered near the walls of the mesopore, together with isotropically rotating molecules located further from the walls seems more likely. This is similar to the case in crystalline Phase II methane, where one molecule per unit cell rotates freely while the others are fixed.[33] The greater disorder in the present system is likely to allow a greater proportion of "free" molecules on one hand, although strong interactions with the walls are likely to cause static molecules to be present in this system to much higher temperatures than in bulk methane. Much more complex modelling would be required in order to determine the exact nature of the rotational diffusion in this system and it is not pursued further in this work. The models for rotational diffusion are all temperature independent, and so do not give any further information concerning the experimentally observed temperature dependence of the EISF.

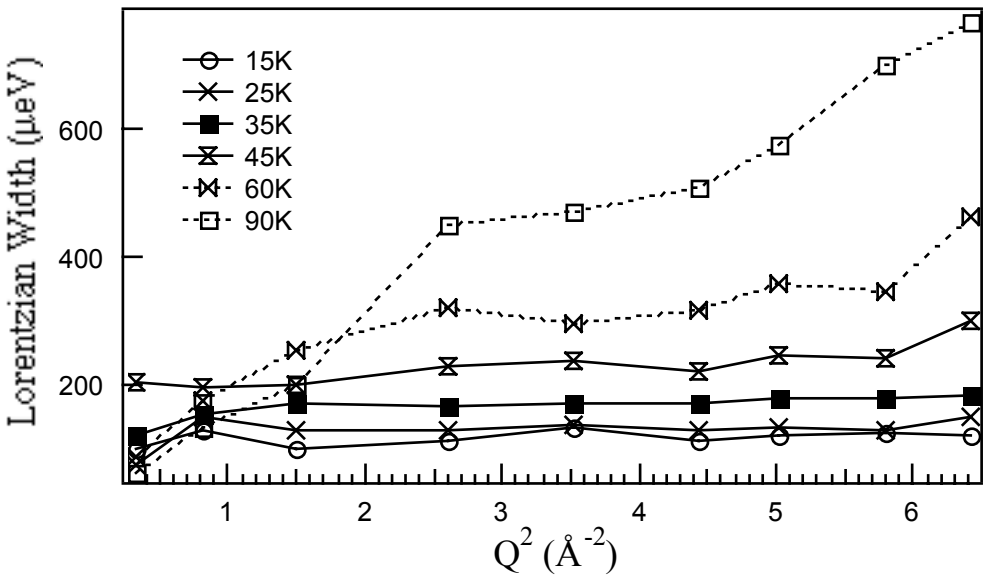

Figure 6.6 *Momentum transfer dependence of the Lorentzian width of the quasielastic scattering from 6.68 mmol g^{-1} of methane adsorbed in MCM-41 at different temperatures.*

Figure 6.6 shows the Q-dependence of the width of the Lorentzian component as a function of temperature. At low temperatures ($15 < T < 45$ K) the Lorentzian width increases slowly with temperature but is essentially independent of Q. These almost Q-independent Lorentzian widths, or more strictly, bounded hydrogen diffusive motions, at low temperatures are characteristic of rotational diffusion of the molecule. An Arrhenius plot, shown in Figure 6.7, of the temperature dependence of these widths gives an Arrhenius law for the correlation time for isotropic rotational diffusion for the temperature region $15 < T < 45$ K of $\tau = 1.5(3)\times10^{-11}$ exp(0.13(4)/RT) sec. The activation energy of 0.13(4) kJ mol^{-1} is, of course, smaller than normally seen for larger molecules.

The rotational activation energy for methane on a graphite caesium intercalate compound ($C_{28}Cs(CH_4)$) was found to be 1.1 kJ mol^{-1} for data in the range 50-160 K[39] which is somewhat higher than observed here. This indicates a greater interaction between the methane and the substrate than exists in the methane-MCM-41 system. Rotational diffusion coefficients for methane in NaY zeolite at 100 K[40] and for methane in ZSM-5 at 200 K[41] have been found to be 4.5×10^{10} s^{-1} and $2.5\text{-}4.2\times10^{10}$ s^{-1} (dependent upon methane loading in the pores) respectively. The values of the rotational diffusion constant in these silicate and aluminosilicate systems are lower than the values obtained for methane adsorbed on graphite (6×10^{11} s^{-1} at 55 K)[42] or in bulk solid methane (10^{12} s^{-1} at 21 K)[43] indicating slower rotation due to interactions of the molecule with the framework. The value of the rotational diffusion constant for methane on MCM-41 of 7×10^{10} s^{-1}, indicates somewhat less hindering of the methane rotation than is observed in the other zeolites.

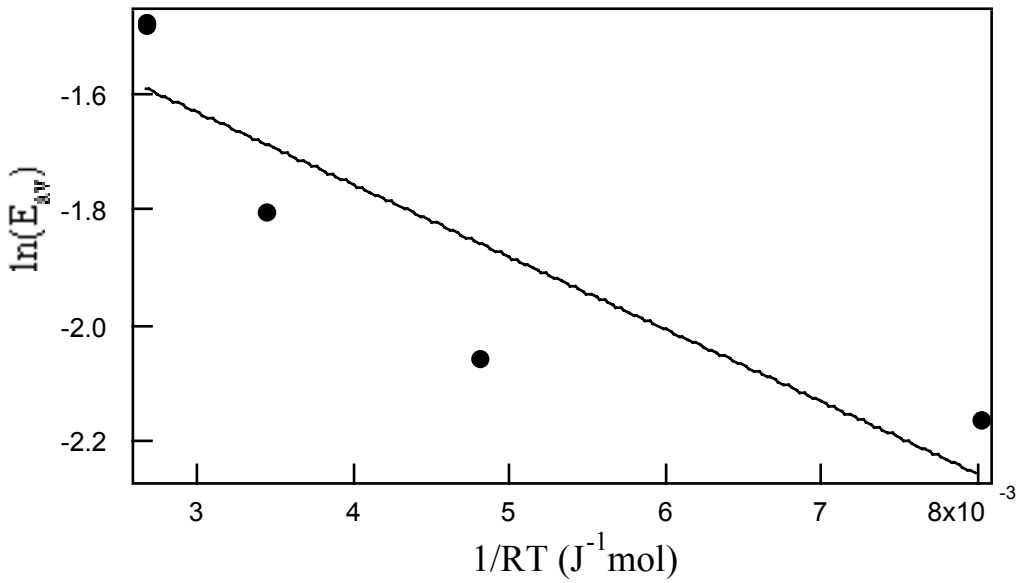

Figure 6.7 *Arrhenius plot of the temperature dependence of the width of the quasielastic scattering for temperatures between 15 and 45 K.*

Above 45 K a strong Q dependence with an approximately Q^2 dependence is observed for the energy widths of the Lorentzian component. This is characteristic of unconfined translational diffusion. Although the statistics are relatively poor this behaviour persists at higher temperatures and there appears to be a component behaving according to this scattering law up to 180 K. The slope of the curves at 60 K and 6.68 mmol g^{-1} in Figure 6.6 imply diffusion constants for long-range translational motion of $4.5(8)\times10^{-6}$ cm^2 s^{-1} and $11.1(8)\times10^{-6}$ cm^2 s^{-1} compared with that of 2.7×10^{-6} cm^2 s^{-1} at the triple point of pure methane at 191 K.[44]

The diffusion constants for all temperatures above 45 K are plotted as a function of inverse temperature in Figure 6.8. For comparison the diffusion constants for methane in various other porous systems at a range of temperatures are also plotted in Figure 6.8. The values were taken from a number of sources, and were measured by QENS,[40,41,45,46] pulsed field gradient nmr[45-48] and through molecular dynamics simulations.[48-50] The translational diffusion constants for MCM-41 appear to be comparable to those for diffusion of methane in silicalite and NaY zeolite for temperatures where the measurements coincide with those for MCM-41.

Given the values at higher temperatures for methane diffusion in the silicalite and NaY systems shown in Figure 6.8, the slope of a plot of diffusion constants with inverse temperature will be quite different from that found for MCM-41. They have a greater slope and thus will have a higher activation energy. From Figure 6.8 the Arrhenius law for the long-range translational diffusion of methane in MCM-41 channels can be derived: $D = 4(2)\times10^{-5} \exp(-1.2(3)/RT)$ cm^2 s^{-1}. The activation energy observed here, 1.2(3) kJ mol^{-1}, is smaller those observed in the other zeolitic systems for which diffusion constants were plotted in Figure 6.7. For methane in ZSM-5, activation energies of 4-5 kJ mol^{-1} were found in the temperature range 200-250 K using both QENS and pulsed field gradient nmr.[46] In silicalite the activation energy for methane translational motions calculated from similar experimental data was 3.9 kJ mol^{-1}.[45] For

methane in NaY zeolite between 100 and 250 K an activation energy of 6.3 kJ mol^{-1} was also found using QENS and pulsed field gradient nmr results.[40] The slightly lower activation energy for translation in MCM-41 may be due to the large amount of empty channel space in the structure, and lack of restrictive cage sites as well as low methane-wall interactions.

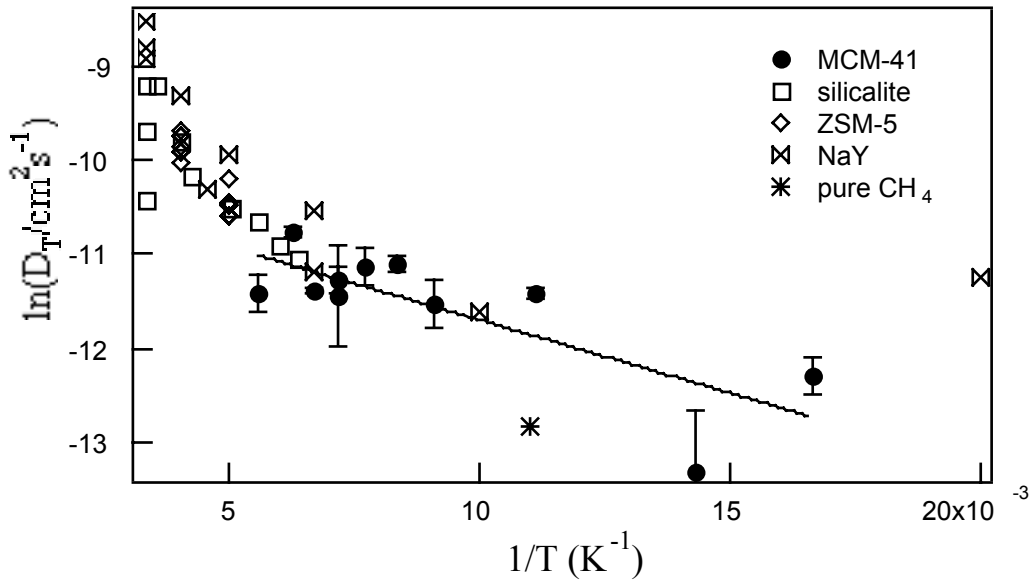

Figure 6.8 *Diffusion constants of methane in MCM-41 pores for temperatures above 45 K compared to values for the diffusion constant of methane in another pure silica system, silicalite,*[45,48] *in aluminosilicate zeolites, ZSM-5*[41,46] *and NaY*[40,47,49,50] *and in bulk methane at 191 K.*[44] *The solid line is a least squares fit to the MCM-41 data.*

It can be concluded that methane diffusion in MCM-41 has a slightly larger rotational diffusion constant and a smaller activation energy for translation than in other, more restrictive zeolite cage materials. The diffusion constants and activation energies are, however, in the expected range, which is quite different to that of pure methane.

6.3 Inelastic Scattering from Methane

The experiment using the machine QENS described above also collected data for methane on MCM-41 in the inelastic scattering region which can be compared to inelastic scattering measurements on bulk methane.

Solid methane II at low temperatures has well developed rotational tunnelling excitations and at 15 K a clear librational excitation at *ca.* 1 millielectron volt.[51] This was verified in the control series of experiments on QENS with bulk methane, but no trace of it was found in the near inelastic region for methane in MCM-41. Figure 6.9 shows the energy transfer region $0 < \delta E < 120$ millielectron volts from MCM-41 containing methane at temperatures between 15 K and 140 K. The inelastic scattering signal is about 100 times weaker than the scattering from the quasielastic region but is persistent. Even at 180 K, where the adsorption isotherm shows there is still plenty of methane present, there is a strong scattering signal of approximately the same intensity as at lower temperatures. For comparison the very weak scattering from empty MCM-

41 is shown. The inelastic scattering is likely to be due to the recoil spectrum for methane within the MCM-41 channels.

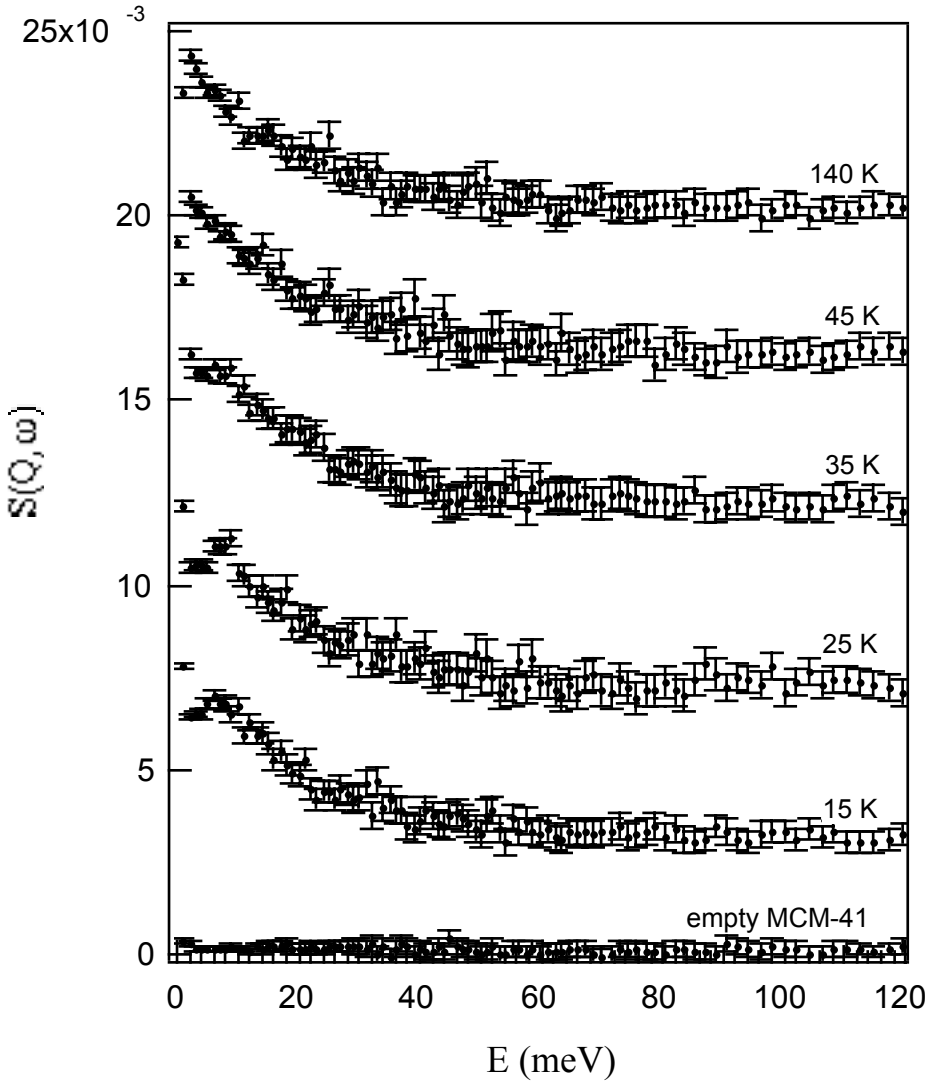

Figure 6.9 *Inelastic scattering from 6.68 mmol g^{-1} of methane adsorbed on MCM-41 at various temperatures, compared to an empty MCM-41 sample at 15 K.*

6.4 Methane Adsorption Isotherms

The adsorption isotherm of methane at 77 K on MCM-41 closely resembles that for nitrogen.[17] Figure 6.10 shows typical comparable isotherms, in this case for material of much improved long range order,[52] following the method of Ryoo and Kim.[53] Surface areas were calculated using molecular areas of 16 Å^2 per molecule for nitrogen[54] and 14.2 Å^2 for methane.[55] The BET surface area available to methane for this material was 760 m^2 g^{-1} while the nitrogen BET surface area was 1160 m^2 g^{-1}.

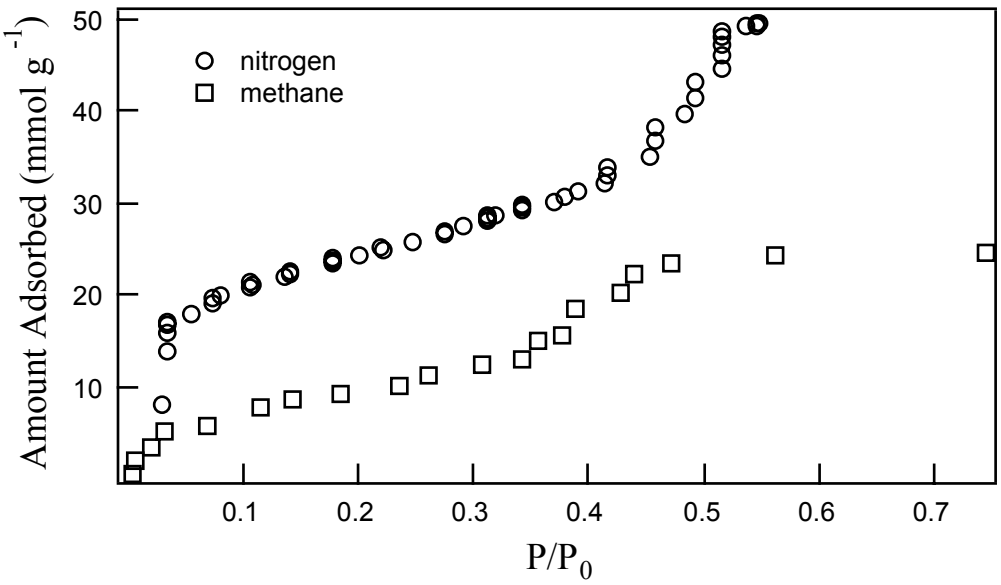

Figure 6.10 *Adsorption isotherms for methane and nitrogen on an MCM-41 sample with high long range order.*

6.5 Discussion

The absence of librational or rotational excitations in methane-filled MCM 41 at energy transfers between about 200 microelectron volts and 10 millielectron volts would not be surprising for temperatures above 25 K, since they are strongly damped in this range of temperature even for solid methane II. The spectra for bulk methane shown in Figure 6.1 at 15 K shows at least the first rotational transition at 1.07 meV although it is not very intense, and although the tunnelling lines cannot be distinguished from the quasielastic peak at this temperature, the peak is broadened and distorted by them. Similar features were, however, not apparent in the methane-filled MCM-41 at the same temperature.

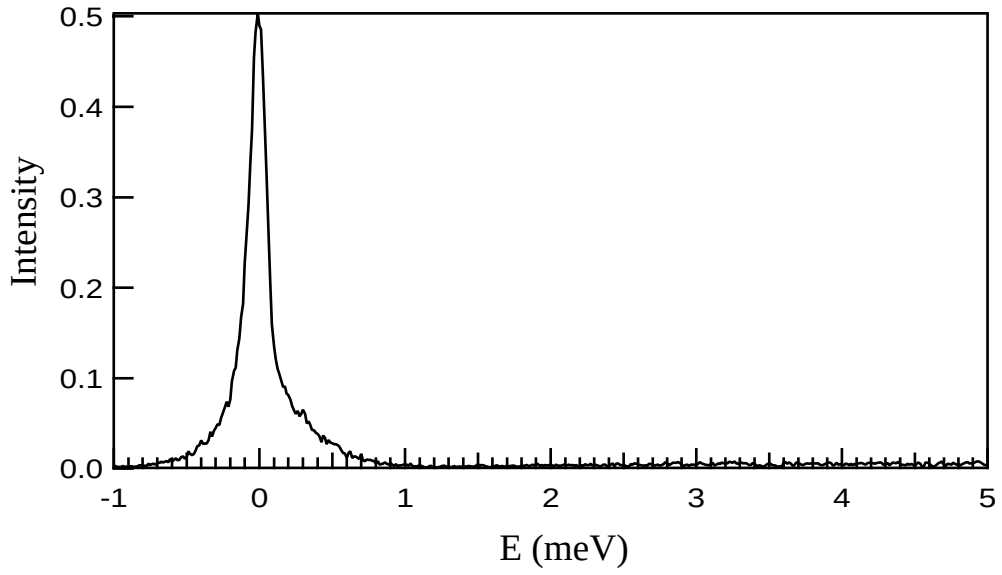

Figure 6.11 *MCM-41 filled with 12.5 mmol g^{-1} of methane at 1.5 K and Q = 2.41 $Å^{-1}$.*

That no clear librations were seen in the experiments for methane adsorbed on MCM-41 even at 1.5 K suggests a distribution of librational and tunnelling states rather than a single well defined set of such excitations. The spectrum for methane filled MCM-41 at 1.5 K is shown in Figure 6.11 below. This points to the incorporated methane being in a glassy or partly ordered state at low temperatures. One explanation is that there is a distribution of packing density from the walls to the core of the tubes, if indeed the tubes are as relatively uniform as the isotherms and other workers have suggested. It may also be explained by having methane adsorbed on a multiplicity of wall sites with different potentials in a highly divided silica matrix.

With these hypotheses in mind the changes seen in the neutron quasielastic peak intensity with temperature between $60 < T < 120$ K (Figure 6.3) can be associated with a melting transition. Some degree of rotational freedom for at least some of the molecules is allowed at lower temperatures. Between 15 and 60 K it appears that around 40% of the methane molecules are stationary, while 60% are undergoing isotropic rotation. It seems logical to conclude that the stationary molecules occupy wall sites, while the mobile ones are contained in the pore region. The proportion of static to mobile molecules is about 1:2. This is similar to the proportions of hindered and unhindered hydrogen adsorbed in MCM-41, which were observed in the experiments described below. A similar situation also exists in crystalline Phase II methane where only one molecule per unit cell is allowed to rotate but here, due to the lack of translational symmetry, the description is less precise. In a model having low density, porous silica walls, an increasing degree of rotational freedom, observed in the increasing Lorentzian widths, with increasing temperature is consistent with molecules in the free pore region becoming active while those nearer the walls experience more hindrance to motion. The drop in intensity between 60 and 120 K would occur where the molecules in wall sites begin to desorb. This model is complex as three types of methane could potentially be present at a single temperature - highly restricted or stationary methane on wall sites, methane with some rotational freedom in pores in the walls, and freely translating methane in the central, empty channel.

As the temperature dependence of the EISF shows, there is a solid to liquid phase transition for at least part of the sample between 60 and 90 K. That it is only some of the methane molecules is suggested by the further evolution of the EISF. Between these temperatures, the EISF shown in Figure 6.4 changes shape, at the higher temperature decreasing continuously but less sharply in the experimental Q region, starting from 0.7 at 0.57 $Å^{-1}$ reaching 0.2 at 2.53 $Å^{-1}$. This suggests that there is still some solid, rotationally active methane present, but that the remainder is now translationally diffusing. As the temperature increases further, the EISF continues to become flatter. Although the interpretation of the EISF when the quasielastic scattering contains both translational and rotational diffusion components in the Lorentzians is more difficult, it is only safe to conclude that above approximately 60 K there is a form of fluid methane present in the MCM-41 cylindrical tubes. This represents a depression of the melting point for this component of nearly 30 K from the bulk value of 91 K. The Lorentzian width data also suggest that at 120 K there is still a well defined fluid component, and so there may also be an elevation of the boiling point from the bulk value of 112 K.[34]

Lastly the results show persistent scattering between 0 and approximately 40 millielectron volts for all samples containing methane at temperatures between 15 K and 140 K. This scattering, shown in Figure 6.9, is probably due to the recoil spectrum of methane within the pores. Even at 140 K there is almost no diminution of the extrapolated limiting intensity at zero energy transfer compared to the data at 15 K or 25 K. The scattering is unlikely to contain enhancement of the empty MCM-41 lattice modes but may involve some interaction between highly dendritic silica and the methane molecules. A more detailed interpretation would require further work over a wide range of momentum transfers.

6.6 Hydrogen in MCM-41

The work on hydrogen adsorbed in MCM-41 covers both inelastic neutron scattering and a detailed analysis of hydrogen adsorption isotherms, compared to those of nitrogen in the same MCM-41 sample. Adsorbed hydrogen is a probe of the tube structure, and, in the fine state of division produced by the tubes, is itself currently of interest.[1,56,57] Hydrogen doped into MCM-41 was examined and data on the dynamics of the adsorbed molecule from inelastic neutron scattering measurements on hydrogen adsorbed into MCM-41 at various temperatures and dopings is reported below.

6.7 Quasielastic & Inelastic Neutron Scattering From Hydrogen

A highly ordered form of MCM-41[52] showing seven orders of the in-plane hexagonal synchrotron X-ray diffraction pattern was used as the substrate (see Figure 5.1 in the previous Chapter). Prior to any experiments, the material was outgassed at 250˚C under a pressure of 10^{-4} torr at 350˚C for two days to remove any residual water in the mesopores. A small quantity of residual hydroxyl groups arising from incomplete siloxyl condensations in the synthesis remained as the only hydrogenous material in the substrate. To remove these, the calcined MCM-41 material was soaked in D_2O to exchange the hydrogen for deuterium. Although the experiment involved doping this deuterium-exchanged material with hydrogen gas, further exchange of the deuterium was unlikely because the low temperature experimental conditions and lack of catalytic material ensured stability of the dihydrogen molecules to both spin conversion (so that spin equilibrium was never reached) and exchange. The sample, weighing 1.10(5) g, was transferred to an aluminium sample can mounted in a cryostat capable of reaching 1.5 K. Hydrogen gas was admitted to the sample in volumetrically determined amounts with an accuracy of *ca.* 2% in volumes, and 2 torr in pressure, which is 0.2% of the highest pressures used.

The quasielastic neutron scattering spectrometer, QENS, at the Intense Pulsed Neutron Source, Argonne National Laboratory (described in Chapter 3) was used for the inelastic neutron scattering experiments. A series of spectra at 1.9 K were taken with hydrogen loadings of 0, 9.5, 12.1, 21.5, 34.5 and 40.3 mmol g^{-1}. Higher temperature spectra were also obtained at 9.8 K (34.5 mmol g^{-1}), 13.3 K (37.7 mmol g^{-1}), 14.7 K (33.1, 40.3 mmol g^{-1}), and 21 K (23.1 mmol g^{-1}). A spectrum is shown in Figure 6.12.

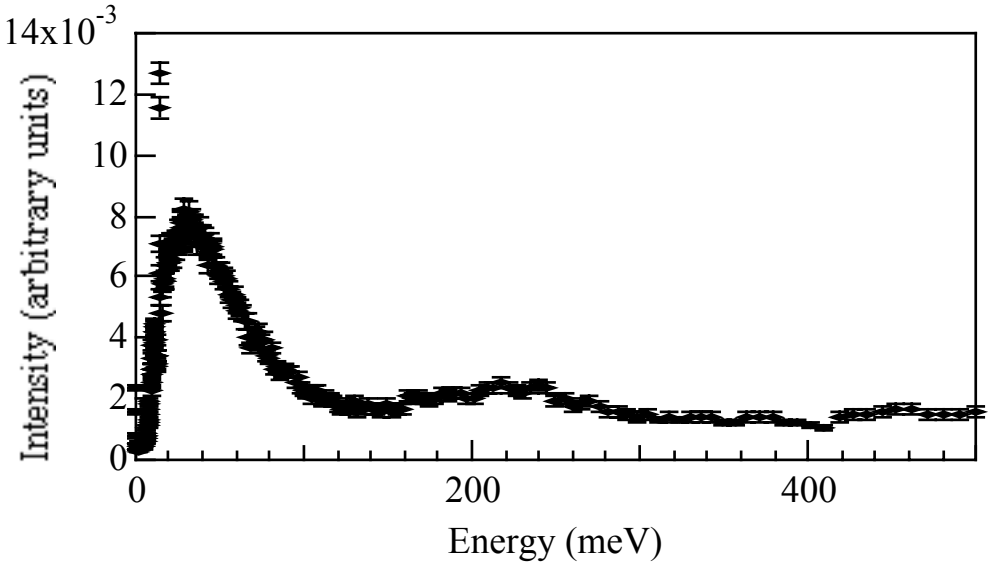

Figure 6.12 *Inelastic neutron scattering from 40.3 mmol g^{-1} hydrogen adsorbed on highly ordered MCM-41 at 1.9 K.*

6.7.1 Results and Discussion

In the experiment discussed in above, the dynamics of methane between 1.5 K and 200 K in filled pores was studied. It was found that this confinement of methane strongly suppresses the normally observable librational excitations of free methane II. It is plausible that the hydrogen case may be the opposite to that of methane. For hydrogen, the high rotational constant and weak interactions may allow observation of molecular rotational dynamics which are modified by the confinement, rather than suppressed. The molecular rotational constant for hydrogen, B = 85.25 K or 7.35 millielectronvolts (meV), is very much greater than the intermolecular potential from the interactions between the molecules in the solid state.

Previous work has shown that hydrogen molecules adsorbed by intercalation compounds[58,59] have rotational tunnelling excitations between about 0.2 and 2 meV while hydrogen at the graphite surface has only weakly hindered rotations at about 12 meV[60] which is comparable to the $J = 0 \rightarrow 1$ transition between free rotor states, at an energy of 14.7 meV. For the intercalates, well defined librational excitations have been observed at energies between 10 meV and 40meV and, even at low temperatures, there is a broad underlying continuum from the molecular recoil scattering.[56] Porous vycor glass (96% SiO_2, 3% B_2O_3[34]) having a nominal pore radius 35 Å filled with *para*-dihydrogen has a strong peak in the inelastic scattering at 14.7 meV and a broad spectrum of scattering present from 15 to 25 meV in measurements taken at 2 and 14 K.[61] The strong peak indicates that the hydrogen is freely rotating within the pores at these temperatures, while the broad band of scattering represents the collective excitations of the liquid or solid phase shifted by the rotational transition. Liquid hydrogen, causing broadening of the quasielastic scattering peak, is present in the vycor pores at 14 K, although not at 2 K. The hydrogen was observed to freeze at 10 K into a solid, unlike bulk solid hydrogen, which freezes around 14 K.

There is no measurable energy broadening of the elastic peak for hydrogen on MCM-41, at any of the observed fillings and temperatures. An upper limit to the broadening is 0.1 meV at a Q of 2.41 $Å^{-1}$, even for the data at 21 K on partially filled samples, or at 14.7 K on fully filled (see section 6.8 for discussion of hydrogen isotherm data). This is far smaller than arises from diffusion in fluid hydrogen,[62] or in vycor pores,[61] indicating that the hydrogen in MCM-41 is much more translationally confined than that in the free fluid or in vycor pores of similar dimensions.

The major feature of the inelastic scattering in the spectrum is a broadly structured continuum to the highest energy transfers measured (Figure 6.12). The first features are relatively sharp peaks at 11.8(2) and 14.7(3) meV (see Figure 6.13 for detail) which can be assigned to $J = 0 \rightarrow 1$ rotational transitions of two types of hydrogen molecules. Above the sharp $J = 0 \rightarrow 1$ peaks the spectrum has a broad peak at 20-30 meV, and further broader, weaker peaks at 180-220 and 400-500 meV. The quoted range reflects not uncertainty in the peak positions, but their variation with scattering angle. The intensity of this continuous spectrum is proportional to the total loading, and thus all hydrogen, both unhindered and weakly hindered contributes to it. Such continuous spectra have been observed in other systems containing hydrogen molecules and hydrogen atoms.[57,58,61,63] They arise from the molecular form factor and the recoil of the hydrogen molecule in the scattering collision which broadens the rotational transitions and allow the effective mass of the scatterer and its mean kinetic energy to be determined. The theoretical result for liquid hydrogen predicts just such a spectrum, with peaks in the observed positions, which, as observed are slightly Q dependent.[64] However a more extensive net of parameters in energy-momentum space would be required to extract reliable values for the dynamical parameters.[56,57]

The $J = 0 \rightarrow 1$ transitions can be used as a probe of the environments of the hydrogen molecules, independent of a calculation of the whole inelastic spectrum. Figure 6.13a(ii) shows the neutron inelastic scattering from the hydrogen in the 21.5 mmol g^{-1} loaded system (where the pores are roughly half filled) at 1.9 K for energy transfers between 0 and 20 meV. The distribution peaks at about 11.8(2) meV which suggests, as with H_2 on graphite, that some of the adsorbed hydrogen is weakly hindered in its rotation. In addition there is a weak peak at 14.7(3) meV characteristic of rotationally unhindered H_2 molecules.[61,65] At higher loadings the intensity of this unhindered peak grows rapidly (Figure 6.13a(i) 40.3 mmol g^{-1} loading). A plot of the intensity of the 14.7 meV peak is linear with loading, but intercepts the zero intensity at a finite loading of 19.7 mmol g^{-1}. The 11.8(2) meV peak is distinctly broader than that at 14.7(3) meV indicating more dispersion in the former sites.

It can be concluded that there are two types of hydrogen present, a weakly rotationally hindered type, in a variety of sites, whose amount can reach 20 mmol g^{-1}; and up to a further 20 mmol g^{-1} of an unhindered species which is adsorbed subsequently. It is natural to assign these to a surface adsorbed species and a bulk-like species. The linearity of the plot of the 14.7 meV peak intensity versus filling indicates that this division into two species is a good model. If there were a continuum of species types then curvature in this plot would be expected.

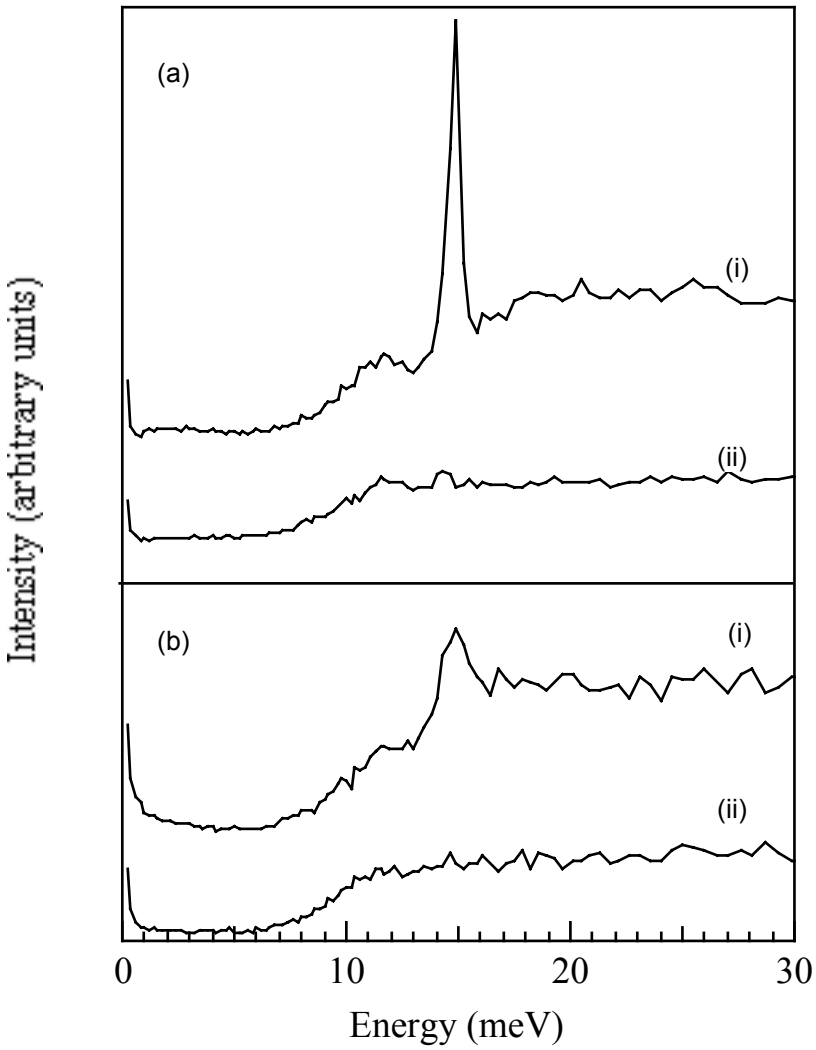

Figure 6.13 *Inelastic neutron scattering from H_2 adsorbed onto MCM-41, 0-30 meV. (a)(i) 40.3 and (ii) 21.5 mmol g^{-1} at 1.9 K; (b)(i) 37.7 mmol g^{-1} at 13.3 K and (ii) 23.1 mmol g^{-1} at 21 K.*

Two species of molecules adsorbed in MCM-41 channels are also seen in ^{1}H NMR experiments on water adsorbed on MCM-41.[22,66] There, three "water phases" were observed. A residual "non-freezing" water is seen at 183 K and is ascribed to silanol groups on the walls of the pores, as well as two phases described respectively as free water within the pores and water bound on the walls. It is likely that the sites so occupied correspond to those occupied by the hydrogen species in this work.

The 14.7 meV peak shows distinct momentum transfer and temperature dependence. Data at three scattering angles was taken, at Q = 2.14, 3.26 and 3.96 Å^{-1}. The highly loaded samples (> 33 mmol g^{-1}) at 1.9 K show a peak width of 0.45(5) meV which is independent of Q, after correction for experimental resolution. Quadrupole-quadrupole interactions, which are very sensitive to the number and distance of nearest neighbours are calculated to give a width of 0.58 meV, independent of Q, in solid, 25% *ortho*-hydrogen, molecular hydrogen.[67] Thus the width observed indicates a nearest neighbour packing of the bulk hydrogen in the pores that is very close to that observed

in the crystal, and much denser than in liquid hydrogen, in which $<1/r^5>$ is 60% of the crystal value. The intensities are given by:

$$I(Q) \propto j_1^2 \left| \frac{Qd}{2} \right| e^{-2W} \qquad \textbf{(6.4)}$$

where $j_1(Qd/2)$ is the spherical Bessel function, d is the distance between the nuclei in a molecule, and e^{-2W} is the Debye-Waller factor. After adjustment for scale factors and the form factor of a proton freely moving on a sphere of radius 0.3707 Å, the intensities therefore show a decrease with Q fitted well by a mean square translational displacement factor ($<U^2>$) of 0.55(5) Å^2. This value is marginally larger than that observed for crystalline hydrogen at 5.4 K of 0.48(3) Å^2, which is attributable to the large zero-point motion in this quantum crystal.[58,68]

This amplitude again indicates a local environment close in density to that of the solid material. At 13.3 K for the 37.7 mmol g^{-1} loading the amplitude increases to 0.7(1) Å^2, and the FWHM of the peak has increased, being 0.9(1), 1.0(1), and 1.2(1) meV at the three scattering angles (Figure 5.5b(i)). At 21 K the 14.7 meV peak is no longer apparent (Figure 5.5b(ii)). The main features are as expected - increase in temperature increases translational thermal motion from values typical of zero-point hydrogen motion, and decreases the lifetime of the rotational states.

6.8 Nitrogen and Hydrogen Adsorption Isotherms

The measurements and analysis in this section were done by Dr. Peter Branton and Dr Philip A. Reynolds. They are included here for completeness, to show the thermodynamic behaviour of the highly ordered MCM-41 materials used.

Considerable thermodynamic data can be derived from adsorption isotherm measurements on MCM-41. Hydrogen adsorption isotherms complement the neutron scattering work reported in the preceding sections, and nitrogen adsorption isotherms were investigated as a control and for comparison with published nitrogen adsorption data on less well ordered MCM-41 materials.[15,17,18,69,70]

Both adsorption and desorption isotherms with hydrogen were performed at low temperature, although, because of the thermal inertia and uncertainty about gas volumes in the sample area they are not of the highest accuracy. They are, however, valuable since they are not easily obtainable with the usual experimental equipment. A complete adsorption isotherm was measured at 21.5 K. The desorption isotherm at 21.5 K was less detailed (Figure 6.14). At 15 K an initial large dose of hydrogen was adsorbed on the MCM-41, and desorption measured in detail at this temperature. Adsorption up to *ca.* 100 torr pressure was also measured at temperatures between 31 and 61 K. Besides their intrinsic interest, these isotherms were used to verify hydrogen loadings at various stages of the neutron experiments. Errors in the temperature readings were of the order of a few tenths of a Kelvin.

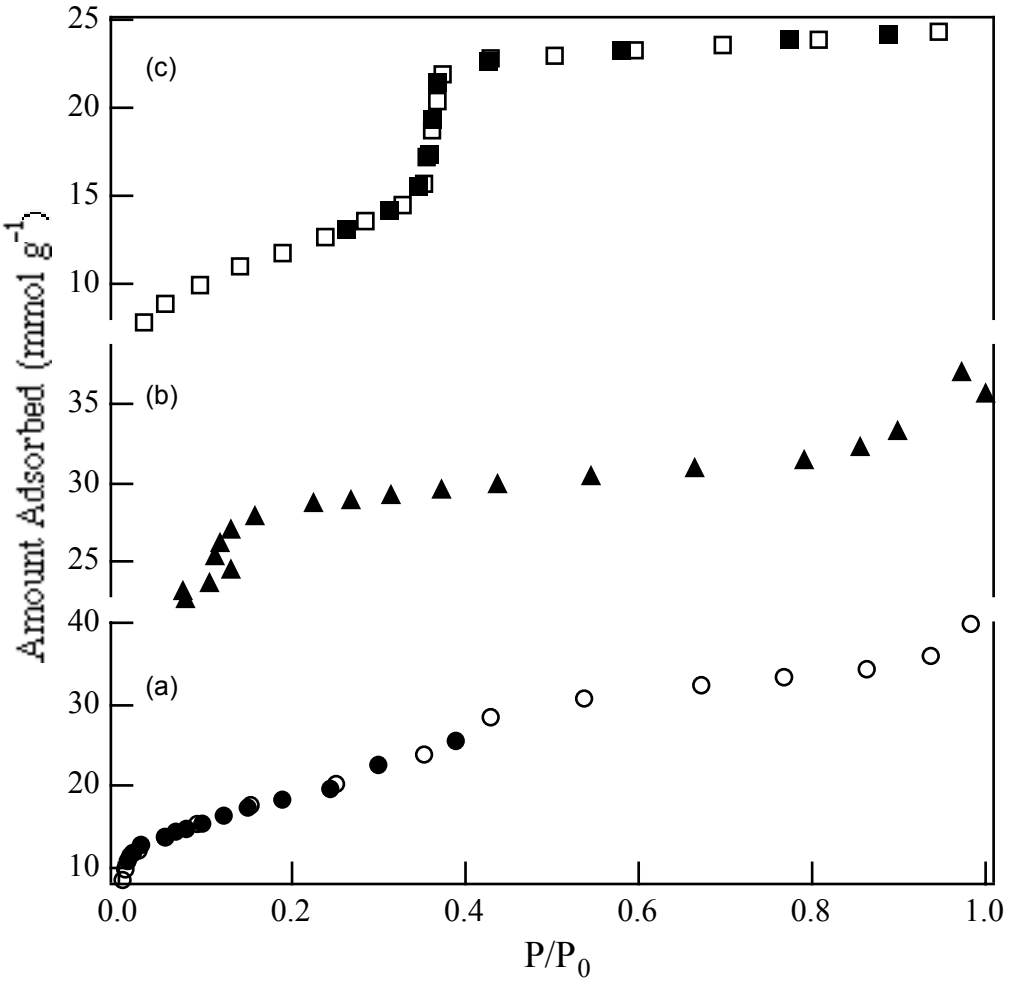

Figure 6.14 *Isotherms of H_2 on MCM-41 (a) at 21.5 K (circles) and (b) at 15.2 K (triangles), and (c) adsorption isotherm of N_2 on MCM-41 at 77K (squares), open symbols denote adsorption, filled symbols denote desorption.*

In the course of adsorption and neutron measurements some interesting thermal behaviour was noticed. For example, at a loading of 34.8 mmol g^{-1}, about 90% of fully filled, upon allowing the sample to warm to 21 K from 2 K, the H_2 vapour pressure increased smoothly and slowly, at *ca* 2 torr min^{-1}, to 48.8 torr. At this pressure, in less than a minute the pressure increased to 318 torr, and then remained relatively stable. However for 27.2 mmol g^{-1} loading, the pressure increase was slow and steady to the final equilibrium pressure at 21 K. This behaviour was observed several times - an apparently first order transition for higher loadings, but for lower loadings (at and below about 50%) this behaviour was suppressed.

6.8.1 Results and Discussion

Adsorption and desorption isotherms of hydrogen on MCM-41 at 21.5 K are shown in Figure 6.14(a), (b). Similar to the nitrogen isotherm (also measured using a volumetric technique) at 77 K and shown in Figure 6.14(c), these are of Type IV in the IUPAC classification.[71] The nitrogen isotherm is completely reversible at 77 K. For the hydrogen isotherm at 21.5 K an insufficient number of desorption points makes it

unclear whether there is small hysteresis or completely reversible capillary condensation-evaporation from the mesopores. The desorption branch at 15 K (Figure 6.14(b)) showed a point of inflection where evaporation occurs at a relative pressure, $P/P_0 = 0.12$, while the same point of inflection occurs on the 21.5 K desorption branch at *ca*. $P/P_0 = 0.4$. Hysteresis is known to be dependent on the temperature; as the critical temperature is approached, theory predicts that any hysteresis will diminish in size and shift towards higher relative pressures.[72,73] Nitrogen adsorption on MCM-41 is a good example of this phenomenon; Ravikovitch *et al*.[15] determined that for a pore spacing of 45 Å, hysteresis was observed at 70.6 K over the pressure range *ca.* 0.34-0.45, but at 77 K no hysteresis was evident and the reversible capillary condensation/evaporation occurred over the range *ca.* 0.38-0.45.

The pore diameter range in Table 6.1 has been estimated by the application of the Kelvin equation (with the usual drastic assumptions such as hemispherical meniscus, zero contact angle and bulk surface tensions) with allowance made for multilayer adsorption on the pore walls.[71,74] The derived values of 13 to 26 Å are smaller than the values derived from the nitrogen isotherm in the same way (28-35 Å), which may reflect the questionable validity of the Kelvin equation when applied to small mesopores.

Values of the BET monolayer capacity, n_m(BET) and the corresponding BET constant, c(BET) in Table 6.1 have been derived from the isotherm data in the usual manner.[71,74] The BET plot was linear over the approximate range, $0.05 < P/P_0 < 0.3$. A surface area, A(BET) of 980 $m^2\ g^{-1}$ was calculated from the BET equation on the nitrogen isotherm over the range $0.05<P/P_0<0.32$ and by assuming the molecular area, a_m, to be 16.2 $Å^2$ in the completed monolayer.[71] If this area is assumed to be the area available for the adsorption of hydrogen, the apparent molecular area, $a_m(1)$, can be calculated from the hydrogen n_m(BET) value. This value of 10.3 $Å^2$ is smaller than the corresponding value, $a_m(2)$=14.4 $Å^2$, calculated from the liquid density[34,54] (*ie*. assuming close-packing, as in the free liquid). The neutron scattering experiments, described above and in Chapter 5, support hydrogen in a solid-like state. By calculating $a_m(2)$ using the density of solid hydrogen, a value of 11.7 $Å^2$ is obtained, in much better agreement with the $a_m(1)$ value of 10.3 $Å^2$. It can thus be deduced that the hydrogen in the pores is more densely packed than in the free liquid and approaches the solid hydrogen density.

Table 6.1 *Pore characteristics from isotherm data.*

Adsorbate	T /K	n_m(BET) /mmol g^{-1}	c(BET)	a_m(1) /Å^2	a_m(2) /Å^2	P/P_0	d_p /Å	V_p /m^3Mg^{-1}
Nitrogen	77	10.0	118	(16.2)	16.2	0.33-0.37	28-35	0.84
Hydrogen	21.5	15.8	94	10.3	$14.4^{(l)}$ $11.7^{(s)}$	0.33-0.44	19-26	$1.02^{(l)}$ $0.75^{(s)}$

a_m(1) is the cross-sectional area calculated from the nitrogen area and the individual value of n_m. a_m(2) is the cross-sectional area calculated from the adsorbate density ($^{(l)}$ refers to liquid and $^{(s)}$ refers to solid hydrogen density). P/P_0 refers to the range of mesopore filling/emptying. d_p is the effective pore diameter obtained by application of the Kelvin equation with allowance made for multilayer adsorption on the pore walls. V_p is the total mesopore volume ($^{(l)}$ assuming adsorbed liquid hydrogen and $^{(s)}$ assuming adsorbed solid hydrogen).

The total mesopore volume, V_p, in Table 6.1, was obtained from the volume adsorbed at $P/P_0 = 0.95$ and assumed that the pores have been filled with condensed liquid adsorptive.[54] It was larger than the value calculated from the nitrogen isotherm. The pore volume was calculated again, assuming that the adsorbed hydrogen was in a solid-like state and, as above, gives clear evidence that the hydrogen in the mesopores has solid-like properties, again supporting the neutron scattering evidence.

Confirmation that chemisorption is not occurring is provided by calculations of the isosteric enthalpy of adsorption, q^{st}. A value significantly greater than the enthalpy of vaporisation of hydrogen, ΔH_l, (0.898 kJ mol^{-1} at 20.3 K),[54] is an indication of chemisorption. Using temperatures between 15 and 50 K, and assuming a monolayer capacity, n_m(BET) of 15.8 mmol g^{-1}, q^{st} varied from *ca*. 3.4 kJ mol^{-1} at $\theta = 0.2$, to *ca*. 1.7 kJ mol^{-1} at $\theta = 0.8$, to *ca*. 1.2 kJ mol^{-1} at $\theta = 2$ (where θ is the surface coverage). The higher q^{st} values below a monolayer surface coverage are consistent with a heterogeneous surface, which has been noted for MCM-41 by other authors.[75] The approximately constant value of q^{st} above a monolayer is only slightly above ΔH_l and thus physisorption only can be inferred.

The fact that all the void space is filled, and that at higher loadings upon warming, a first order transition, assignable to a boiling transition, is observed, suggests the possibility that the hydrogen is filling a single connected void volume. This agrees with the contrast variation SANS results from water in calcined MCM-41, discussed in Chapter 5 which show all voids filled. If different mesopores vary in properties, it might be expected that the hydrogen within them would boil, if it does, at slightly different temperatures, so that the phase transition would occur over time-scales of minutes rather than seconds. The observation suggests either that *all* the mesopores are coupled and behave collectively or the mesopores are remarkably uniform, considering the amorphous nature of the silica. By implication this suggests that there are significant void connections through the walls between different mesopores. At lower

loadings the hydrogen aggregations become disconnected and there is no single boiling point, indicating, at a minimum, that different mesopores are no longer influencing each other.

6.9 Conclusions

Methane in completely filled MCM-41 channels does not behave like bulk methane. The major component of the sample shows isotropic rotational diffusion of some of the methane between 15 and 60 K, although around 40% of the molecules are stationary at these temperatures. This is followed by a liquefaction transition above 60 K. The extent of melting has not been determined but it seems that liquid is present at 120 K and a persistent fluid up to 180 K. This indicates a smearing in temperature of both melting and boiling of the methane in the mesoporous tubes compared to bulk methane.

The inelastic neutron scattering from hydrogen in MCM-41 shows the spectrum characteristic of the hydrogen molecule recoil spectrum. However at low energy transfers, because the momentum transfer is low enough, discrete H_2 molecule rotational J = 0 -> 1 transitions are observed. At lower fillings a somewhat broadened peak at 11.8(2) meV is seen, corresponding to physisorbed molecules on a range of surface sites. At higher coverages a sharp 14.7(3) meV peak is observed, corresponding to H_2 molecules surrounded by others. These two types are sharply differentiated, with little intermediate, and in the fully filled MCM-41 are in the molar ratio 1:1. The translational thermal motion observed in the intensity of the 14.7 meV peaks, the small value of diffusion indicated by lack of quasielastic scattering, and the peak width, indicate that the bulk-like molecules are solid rather than liquid-like in density and packing up to 14 K.

Agreement of hydrogen adsorption isotherms with nitrogen adsorption data is obtained if it is assumed that the hydrogen in the pores is 20% denser than the free liquid, more like that of the free solid, giving surface area and pore volume of 0.75 $cm^3\ g^{-1}$ and 1110 $m^2\ g^{-1}$ respectively. The observed isosteric heats of adsorption show an initially very heterogeneous surface, varying from 3.4-1.7 kJ mol^{-1} at low surface coverages between 0.2 and 0.8. As the hydrogen coverage increases above a monolayer amount, the heat, as expected, decreases towards the enthalpy of vaporisation of liquid hydrogen (0.9 kJ mol^{-1}) being 1.2 kJ mol^{-1} just before free liquid condenses. At higher fillings, on warming the sample, a first order transition apparently due to all the sample hydrogen simultaneously boiling indicates that the array of hexagonally packed MCM-41 tubes may be a single interconnected void. This implies significant voids penetrating the walls between the tubes. This collective behaviour is suppressed at lower fillings.

6.10 References

1. L.S. Bartell, *J. Phys. Chem.,* **1995**, *99*(4), 1080-1089.
2. E.M. Piotrovskaya and E.N. Brodskaya, *Langmuir,* **1995**, *11*(6), 2121-2124.
3. D. Nicholson, *J. Chem. Soc., Faraday Trans.,* **1996**, *92*(1), 1-9.
4. R. Ryoo, C.H. Ko, J.M. Kim and R. Howe, *Catal. Lett.,* **1996**, *37,* 29-33.
5. U. Junges, W. Jacobs, I. Voigt-Martin, B. Krutzsch and F. Schüth, *J. Chem. Soc., Chem. Commum.,* **1995**, 2283-2284.
6. A. Jentys, N.H. Pham, H. Vinek, M. Englisch and J.A. Lercher, *Microporous Mater.,* **1996**, *6*(1), 13-17.
7. K.R. Kloetstra, M. van Laren and H. van Bekkum, *J. Chem. Soc., Faraday Trans.,* **1997**, *93*(6), 1211-1220.
8. R. Burch, N. Cruise, D. Gleeson and S.C. Tsang, *J. Chem. Soc., Chem. Commun.,* **1996**, 951-952.
9. C.-G. Wu and T. Bein in *Zeolites and Related Microporous Materials: State of the Art 1994.*; Stud. Surf. Sci. Catal., (Eds. J. Weitkamp, H.G. Karge, H. Pfeifer and W. Hölderich), Elsevier Science B.V., **1994**, *Vol. 84A*, 243-250.
10. C.-G. Wu and T. Bein, *Science,* **1994**, *266*, 1013-1015.
11. C.-G. Wu and T. Bein, *Science,* **1994**, *264*, 1757-1759.
12. T. Abe, Y. Tachibana, T. Uematsu and M. Iwamoto, *J. Chem. Soc., Chem. Commun.,* **1995**, 1617-1618.
13. P.L. Llewellyn, U. Ciesla, R. Stadler, F. Schüth and K.K. Unger in *Zeolites and Related Microporous Materials: State of the Art 1994.*; Stud. Surf. Sci. Catal., (Eds. J. Weitkamp, H.G. Karge, H. Pfeifer and W. Hölderich), Elsevier Science B.V., **1994**, *Vol. 84A*, 2013-2020.
14. H.L. Frisch and J.E. Mark, *Chem. Mater.,* **1996**, *8*(8), 1735-1738.
15. P.I. Ravikovitch, S.C.O. Domhnaill, A.V. Neimark, F. Schüth and K.K. Unger, *Langmuir,* **1995**, *11,* 4765-4772.
16. V.Y. Gusev, X. Feng, Z. Bu, G.L. Haller and J.A. O'Brien, *J. Phys. Chem.,* **1996**, *100*(6), 1985-1988.
17. P.J. Branton, P.G. Hall and K.S.W. Sing, *J. Chem. Soc., Chem Commun.,* **1993**, 1257-1258.
18. P.J. Branton, P.G. Hall, K.S.W. Sing, H. Reichert, F. Schüth and K.K. Unger, *J. Chem. Soc., Faraday Trans.,* **1994**, *90*(19), 2965-2967.
19. C.-Y. Chen, S.-Q. Xiao and M.E. Davis, *Microporous Mater.,* **1995**, *4*(1), 1-20.
20. C.-Y. Chen, H.-X. Li and M.E. Davis, *Microporous Mater.,* **1993**, *2,* 17.
21. J.S. Beck, J.C. Vartuli, W.J. Roth, M.E. Leonowicz, C.T. Kresge, K.D. Schmitt, C.T.-W. Chu, D.H. Olson, E.W. Sheppard, S.B. McCullen, J.B. Higgins and J.L. Schlenker, *J. Am. Chem. Soc.,* **1992**, *114,* 10834-10843.
22. E.W. Hansen, M. Stöcker and R. Schmidt, *J. Phys. Chem.,* **1996**, *100*(6), 2195-2200.
23. A. Hüller, M.V. Smalley, R.K. Thomas and J.W. White, *Mol. Phys.,* **1981**, *44,* 533.
24. Z. Tan and K.E. Gubbins, *J. Phys. Chem.,* **1992**, *96,* 845.
25. J.Z. Larese and Q.M. Zhang, *Phys. Rev. B,* **1995**, *51,* 17023.
26. A. Inaba, J. Skarbek, J.R. Lu, R.K. Thomas, C.J. Carlile and D.S. Sivia, *J. Chem. Phys.,* **1995**, *103,* 1627.

27. R.P. Humes, M.V. Smalley, T. Rayment and R.K. Thomas, *Can. J. Chem.,* **1988**, *66,* 557.
28. J.S. Beck, C.T.-W. Chu, I.D. Johnson, C.T. Kresge, M.E. Leonowicz, W.J. Roth and J.C. Vartuli, *US Patent, No. 5,108, 725,* **1992**.
29. M. Bée, *Quasielastic Neutron Scattering*, Adam Hilger, Bristol, **1988**.
30. Y.D. Harker and R.M. Brugger, *J. Chem. Phys.,* **1967**, *46*(6), 2201-2208.
31. H. Kapulla and W. Gläser in *Inelastic Scattering of Neutrons in Solids and Liquids*; IAEA, Vienna, **1973**, 841-849.
32. W. Press and A. Kollmar, *Solid State Commun.,* **1975**, *17*(4), 405-408.
33. B. Asumussen in *ILL Annual Report*; Grenoble, **1993**, 100-102.
34. *CRC Handbook of Chemistry and Physics*; 75th ed., (D.R. Lide, Ed.), CRC Press, Boca Raton, **1994**.
35. F. Guillaume, J. Doucet, C. Sourisseau and A.J. Dianoux, *J. Chem. Phys.,* **1989**, *91*(4), 2555-2567.
36. W.W. Kagunya, *J. Phys. Chem.,* **1996**, *100*(1), 327-330.
37. F.R. Trouw, *Spectrochimica Acta,* **1992**, *48A*(3), 455-476.
38. A.J. Leadbetter and R.E. Lechner in *The Plastically Crystalline State (Orientationally-Disordered Crystals)*; (Ed. J.N. Sherwood), John Wiley & Sons, Chichester, **1979**, 285-320.
39. F.R. Trouw and J.W. White, *J. Chem. Soc., Faraday Trans.,* **1988**, *84*(7), 861-884.
40. H. Jobic, M. Bée and G.J. Kearley, *J. Phys. Chem.,* **1994**, *98*(17), 4660-4665.
41. H. Jobic, M. Bée and G.J. Kearley, *Zeolites,* **1989**, *9,* 312-317.
42. P. Thorel, J.P. Coulomb and M. Bienfait, *Surf. Sci.,* **1982**, *114,* L43.
43. T. Springer, *Springer Tracts in Modern Physics*, Springer, Berlin, **1972**, *Vol. 64*.
44. P.A. Egelstaff, *An Introduction to the Liquid State*; 2nd ed., Clarendon Press, Oxford, **1992**, 263.
45. P. Demontis, G.B. Suffritti, E.S. Fois and S. Quartieri, *J. Phys. Chem.,* **1992**, *96*(3), 1482-1490.
46. H. Jobic, M. Bée, J. Caro, M. Bülow and J. Kärger, *J. Chem. Soc., Faraday Trans. 1,* **1989**, *85*(2), 4201-4209.
47. J. Kärger and H. Pfiefer, *Zeolites,* **1987**, *7,* 90.
48. A.K. Nowak, C.J.J. den Ouden, S.D. Pickett, B. Smit, A.K. Cheetham, M.F.M. Post and J.M. Thomas, *J. Phys. Chem.,* **1991**, *95*(2), 848-854.
49. S. Yashonath, P. Demontis and M. Klein, *Chem. Phys. Lett.,* **1988**, *153*(6), 551-556.
50. S. Yashonath, P. Demontis and M.L. Klein, *J. Phys. Chem.,* **1991**, *95*(15), 5881-5889.
51. W. Press, *Single Particle Rotations in Molecular Crystals*, Springer, Berlin, **1981**.
52. K.J. Edler and J.W. White, *Chem. Mater.,* **1997**, *9*(5), 1226-1233.
53. R. Ryoo and J.M. Kim, *J. Chem. Soc., Chem. Commun.,* **1995**, 711-712.
54. S.J. Gregg and K.S.W. Sing, *Adsorption, Surface Area and Porosity*; 2nd ed., Academic Press, New York, **1982**.
55. P. Dutta, S.K. Sinha and P. Vora in *Ordering in Two Dimensions*; (Ed. S.K. Sinha), North Holland Publishers, **1980**, 169.

56. G.J. Kellogg, P.E. Sokol and J.W. White in *Momentum Distributions*; (Eds. R.N. Silver and P.E. Sokol), Plenum Press, New York & London, **1990**, 351-354.
57. G.J. Kellogg, J.W. White, K.W. Herwig and P.E. Sokol, *J. Chem. Phys.,* **1990**, *93*(10), 7153-7162.
58. W.J. Stead, P. Meehan and J.W. White, *J. Chem. Soc., Faraday Trans. II,* **1988**, *84*(10), 1655-1668.
59. I.P. Jackson, J. McCaffrey, W.J. Stead and J.W. White, *J. Chem. Soc., Faraday Trans. II,* **1988**, *84*(10), 1669-1682.
60. M. Nielson and W.D. Ellenson, *Annual Report Physics Dept., AEK, Risø,* **1975**, *Report No. 334,* 44.
61. P.E. Sokol, R.T. Azuah, M.R. Gibbs and S.M. Bennington, *J. Low Temp. Phys.,* **1996**, *103*(1/2), 23-33.
62. P.A. Egelstaff, *Proc. Phys. Soc.,* **1966**, *90,* 681.
63. F. Fillaux, R. Papoular, A. Lautie, S.M. Bennington and J. Tomkinson, *International Conference on Neutron Scattering, Sendai,* **1994**.
64. J.A. Young and J.U. Koppel, *Phys. Rev. 3A,* **1964**, *135*, 603-611.
65. W. Langel, D.L. Price, R.O. Simmons and P.E. Sokol, *Phys. Rev. B,* **1988**, *38*(16), 11275-11283.
66. E.W. Hansen, R. Schmidt, M. Stöcker and D. Akporiaye, *J. Phys. Chem.,* **1995**, *99,* 4148-4154.
67. R.J. Elliott and W.M. Hartmann, *Proc. Phys. Soc.,* **1967**, *90.* 671.
68. M. Nielsen, *Phys. Rev. B,* **1973**, *7*(4), 1626-1635.
69. O. Franke, G. Schulz-Ekloff, J. Rathousky, J. Stárek and A. Zukal, *J. Chem. Soc., Chem. Commun.,* **1993**, 724-725.
70. J. Rathousky, A. Zukal, O. Franke and G. Schulz-Ekloff, *J. Chem. Soc., Faraday Trans.,* **1994**, *90*(18), 2821-2826.
71. K.S.W. Sing, D.H. Everett, R.A.W. Haul, R.A. Pierotti, J. Rouquerol and T. Siemieniewska, *Pure & Appl. Chem.,* **1985**, *57*(4), 603-619.
72. A. Keizer, T. Michalski and G. Findenegg, *Pure & Appl. Chem.,* **1991**, *63,* 1495.
73. W.D. Machin, *Langmuir,* **1994**, *10,* 1235.
74. S. Brunauer, P.H. Emmet and E. Teller, *J. Am. Chem. Soc.,* **1938**, *60,* 309.
75. P.J. Branton, P.G. Hall, M. Treguer and K.S.W. Sing, *J. Chem. Soc., Faraday Trans.,* **1995**, *91,* 2041.